Microporous Polymers

DOI: 10.1002/anie.201207163

Surface Area Control and Photocatalytic Activity of Conjugated Microporous Poly(benzothiadiazole) Networks**

*Kai Zhang, Daniel Kopetzki, Peter H. Seeberger, Markus Antonietti, and Filipe Vilela**

Π-conjugated microporous polymers, such as organic semiconductors with additional porosity in the nanorange, are versatile materials.[1] In addition to typical applications for high-surface-area materials, such as gas separation[2] and storage,[2,3] conjugated polymer networks are also potential heterogeneous catalysts[4] and can be used in optoelectronics[5] and for energy applications.[6] Given the importance of surface area and porosity, a simple methodology to influence these parameters is needed. In order to use conjugated polymer networks as catalysts and catalyst supports their chemical stability needs to be improved. Therefore we designed a stable, fully conjugated network by linking benzothiadiazole as a strong electron-withdrawing moiety through three C_{sp}–C_{sp} bonds to benzene as a weak electron-donating component. The surface area of these novel conjugated microporous polymer networks could be adjusted by a simple synthetic protocol.

Benzothiadiazole monomers have proven great stability towards oxidation in photovoltaic applications.[7] The low-band-gap character, high absorption coefficient, and suitable energy levels of benzothiadiazole result in a very strong acceptor to be used in optoelectronic materials, such as low-band-gap polymers,[7,8] non-fullerene acceptors,[9] or n-type field effect transistors.[10] The combination of weak electron donors, such as a phenyl group with benzothiadiazole, may prevent a fast recombination of excitons and increase the yield of intersystem crossing to the triplet state of the polymer, thereby rendering it suitable for photosensitizing.

Conjugated linear polymers with backbones based on the poly(phenylene ethynylene) structure[11] or the polythiophene–porphyrin dyad[12] repeat unit can generate singlet oxygen in water upon irradiation. Singlet oxygen is used for a number of applications, such as for treatment of waste water or in the synthesis of fine chemicals.[13] An industrial process carried out on a scale of several tons a year is the photochemical oxidation of citronellol to rose oxide.[14] Different dyes and transition metal complexes can generate singlet oxygen upon irradiation, and these sensitizers can be used in homogeneous solution or immobilized on a solid support. Working under heterogeneous conditions allows for easy separation of the sensitizer after reaction and reusability. Traditional systems suffer however from quenching of the produced singlet oxygen by the solid support, which reduces the quantum yield.[15] Incorporation of a photosensitizing structure into a polymer backbone is particularly attractive, because no support to immobilize the sensitizer is needed when an insoluble photoactive polymer network is used. Therefore the ability of the conjugated microporous polymer (CMP) network to act as a singlet oxygen photosensitizer was evaluated by employing the oxidation of α-terpinene to ascaridole. The pore size and structure as well as specific surface area are beneficial in providing a high accessibility of exited solid polymer for solubilized oxygen, thus resulting in high efficiency for singlet oxygen generation in dependence of the pore architecture.

A series of polymer networks based on benzothiadiazole as building block was synthesized through palladium-catalyzed Sonogashira–Hagihara cross-coupling polycondensation of 4,7-dibromobenzo[c][1,2,5]thiadiazole with 1,3,5-triethynylbenzen (Scheme 1).

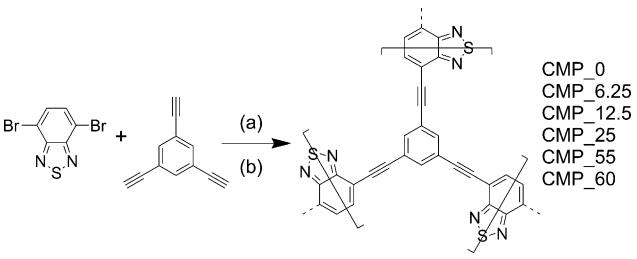

Scheme 1. Synthesis of microporous polymer networks by using SiO_2NPs for surface area control. Reagents and conditions: a) $[PdCl_2(PPh_3)_2]$, CuI, DMF, Et_3N, SiO_2NPs (6.25, 12.5, 25.0, 55, and 60 mg mL^{-1} for CMP_6.25, CMP_12.5, CMP_25, CMP_55, and CMP_60, respectively), 80 °C, overnight. b) NH_4HF_2, H_2O, overnight.

CMP_0 was synthesized in the absence of templating agent, whereas different concentrations of silica nanoparticles (SiO_2NP, $d \approx 12$ nm) were dispersed in the reaction mixtures to produce networks CMP_6.25, CMP_12.5, CMP_25, CMP_55, and CMP_60 (X in CMP_X indicates the amount of SiO_2NPs in mg mL^{-1} used for templating). The reaction mixture became too viscous for the coupling reaction to be completed at concentrations above 60 mg mL^{-1} SiO_2NPs. An aqueous solution of ammonium hydrogen difluoride was used to dissolve the SiO_2NPs after condensation without compromising the polymer networks. The polymers were obtained as dark yellow powders that were completely insoluble in all

[*] Dr. K. Zhang, Dr. D. Kopetzki, Prof. Dr. P. H. Seeberger, Prof. Dr. M. Antonietti, Dr. F. Vilela
Max Planck Institute of Colloids and Interfaces
Am Mühlenberg 1, 14424 Potsdam (Germany)
E-mail: filipe.vilela@mpikg.mpg.de

[**] The Max Planck Society is acknowledged for financial support. We would like to thank Dr. Jérôme Roeser and Prof. Xinchen Wang for the solid-state NMR experiments.

Supporting information for this article is available on the WWW under http://dx.doi.org/10.1002/anie.201207163.

solvents investigated. By using the same amount of starting compounds, all CMPs prepared in the presence of SiO_2NPs were obtained with similar recoveries as for CMP_0, thus showing that the templating agent does not have a detrimental effect on the cross-coupling reaction efficiency. The resulting polymer networks were characterized by elemental analysis, solid-state ^{13}C CP/MAS NMR, N_2 gas sorption, UV/Vis, FTIR spectroscopy, SEM, and TEM.

In the absence of SiO_2NPs, CMP_0 shows carbon signals at around $\delta = 130$ and 122 and 115 ppm, which can be ascribed to the carbon atoms of the phenyl rings (Figure S1 in the Supporting Information). The signals at about $\delta = 95$ ppm can be ascribed to the carbon atom next to the phenyl ring of the −C≡C− group and the signal at approximately $\delta = 87$ ppm to the carbon atom next to the benzothiadiazole unit, a known strong electron acceptor that shifts the carbon peak upfield. CMP_55 was obtained by using a very large amount of SiO_2NPs and shows very similar carbon signals as CMP_0. This indicates that under the harsh conditions required for SiO_2NP removal using ammonium hydrogen difluoride, the chemical structure essentially stays unaffected.

The FTIR spectrum of CMP_60 with SiO_2NPs shows a large SiO_2 signal at 1051 cm^{-1}, which disappeared completely after removal of the SiO_2NPs (Figure 1 b). The spectra of the polymer networks after removal of SiO_2NPs exhibit stretching modes similar to CMP_0. From 2900 to 3400 cm^{-1} C-H stretching bands appear. A C=C stretching mode at 1600 cm^{-1} is observed. All networks show the typical C≡C stretching mode at about 2200 cm^{-1}.

The conjugated polymer networks were dispersed in DMF to obtain UV/Vis spectra (Figure 1 a). They show mainly two absorption maxima at about 320 and 440 nm. Compared to the benzothiadiazole monomer, with absorption maxima at 313 and 350 nm, the polymer networks exhibit a large bathochromic shift of around 90 nm. This indicates the effective enlargement of the π-conjugated system through the polycondensation reaction. Owing to the strong light scattering within the dispersion the absorption edge cannot be easily determined, and therefore the optical band gap cannot be easily estimated. Cyclic voltammetry of thin CMP films was also performed (Figure S12 in the Supporting Information). Quasi-reversible oxidation and reduction cycles were exhibited, which is similar to linear structures based on benzothiadiazole and ethynylbenzene oligomers.[16] HOMO–LUMO band gaps of about 2.10 eV can be calculated.

BET surface areas and pore size distributions were measured for nitrogen adsorption and desorption at 77.3 K (Table S2 in the Supporting Information), and the adsorption isotherms were determined (Figure S10 in the Supporting Information). The BET surface areas range from 270 $m^2 g^{-1}$ in the absence of SiO_2NPs (CMP_0) to 660 $m^2 g^{-1}$ for a large excess of 60 mg mL^{-1} SiO_2NPs (CMP_60).

The BET surface area increases linearly with the concentration of silica nanoparticles in the reaction mixture (Figure 2 a), thereby proving that this is a simple and efficient methodology to control surface area whilst retaining the optoelectronic and chemical characteristics of the polymer. For all networks, similar pore radii in a range from 6 to 8 Å are determined (Figure S10 in the Supporting Information).

Likewise, the total pore volumes ($V_{pore/total}$) of the polymer networks show a clear trend. Without using SiO_2NPs, polymer network CMP_0 exhibits a total pore volume of 0.288 $cm^3 g^{-1}$.

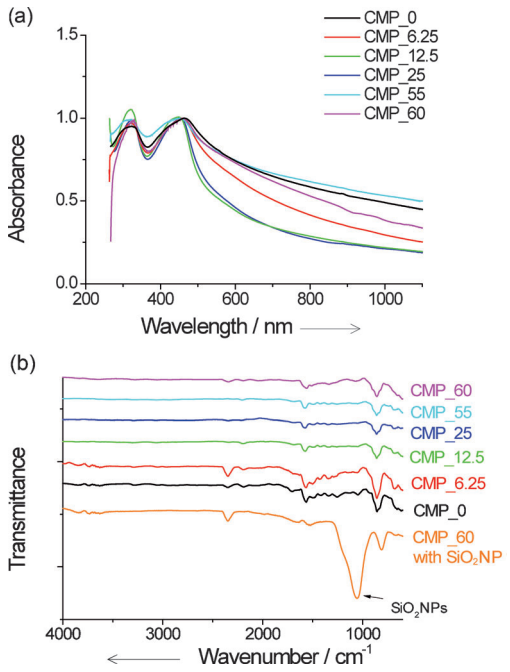

Figure 1. a) UV/Vis spectra of the polymer networks (dispersed in DMF). b) FTIR spectra of the polymer networks CMP_0–CMP_60 and CMP_60 with SiO_2NPs.

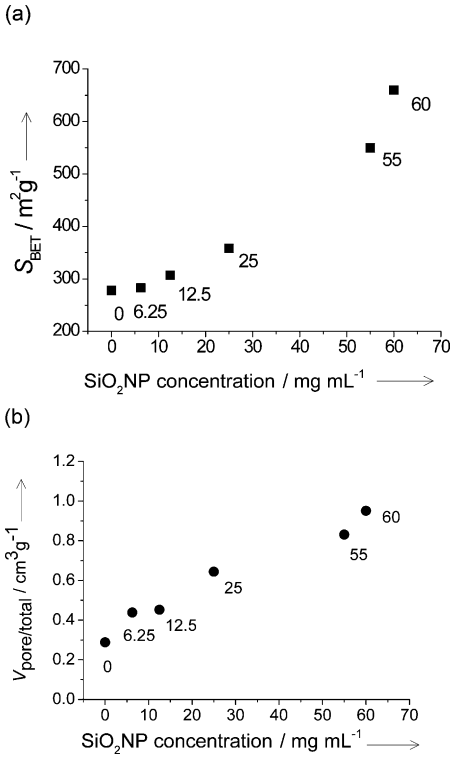

Figure 2. a) BET surface areas of the polymer networks using different SiO_2NP concentrations. b) Total pore volumes of CMP_0–CMP_60.

When employing SiO_2NPs, similar to the effect on the surface area, the $V_{pore/total}$ also increases to 0.951 $cm^3 g^{-1}$ for CMP_60 (Figure 2b). Note that the so-called total pore volume does not contain the silica pores, which are out of the range of these measurements, that is, it is a total micropore volume.

These data suggest that during the coupling reaction of the monomers, the cross-linked polymers are covering the surface of SiO_2NPs, leaving the pore space after template removal. The micropore size in the polymer network obtained did not change, which can be proven by BET surface area measurements of the CMPs before removal of SiO_2NPs, exhibiting always BET surface areas of about 250 $m^2 g^{-1}$. After removal of SiO_2NPs, the micropores simply become more accessible through the big silica mesopores, showing increasing surfaces area and total pore volumes.

This methodology of using SiO_2NPs is presumably not only a simple "templating" effect, since the SiO_2NPs also interfere with the mesostructure formation of the original polymer as observed by electron microscopy. SEM images show clearly distinct polymer morphologies (Figures S8 and S9 in the Supporting Information). CMP_0 depicts a more fibrous morphology, whereas CMP_6.25–CMP_60 are determined by aggregated smaller spheres to form a porous structure. The SiO_2NPs in the reaction mixture inhibit the formation of the fiber-shaped structure as for CMP_0, presumably by suppressing homo-aggregation of precondensed oligomers. TEM images of CMPs with SiO_2NPs display domains of different sizes. The polymer networks are either around or inbetween SiO_2NP assemblies.

The photoenergetical states of the CMPs were investigated by using fluorescence spectroscopy. Interestingly, they did not show any fluorescence. This indicates that the CMPs could transform into a triplet state under excitation with a strong intersystem-crossing process within the conjugated system. Another explanation could be deep traps for one of the photogenerated charges, thus resulting in effective exciton splitting and charge stabilization. In case of strong intersystem-crossing, the polymer in the triplet state might excite triplet oxygen and thus could be employed as photosensitizer. Photophysical studies are however necessary to fully understand these events. This is work currently under investigation and will be the focus of a future publication.

To investigate the feasibility of a CMP network being applied as a heterogeneous photocatalyst in the production of singlet oxygen, a dispersion of cross-linked polymer (1 $mg mL^{-1}$) containing α-terpinene (0.1M) was mixed with oxygen (2 equiv) and pumped through a photoreactor consisting of FEP-tubing wrapped around a polycarbonate plate that was irradiated with blue light at 420 nm (Figure S7 in the Supporting Information; FEP = fluorinated ethylene propylene). This efficient continuous flow setup ensures high throughput at short residence time.[17] The substrate conversion was evaluated by ^{1}H NMR spectroscopy using polymers of various surface areas (Figure 3). At a flow rate of 1 $mL min^{-1}$, CMP_0 gave the lowest conversion (26%), whilst CMP_6.25 through to CMP_55 seem to have reached a plateau in the reaction conversion (70–80%, Figure 3 and Table S3 in the Supporting Information). With CMP_60, the

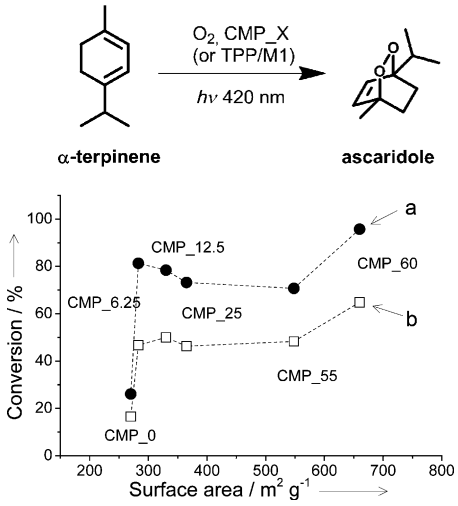

Figure 3. Conversion of α-terpinene into ascaridole with CMPs of different surface areas. a) Flow of oxygen (2 equiv): 5 $mL min^{-1}$, flow of α-terpinene solution: 1 $mL min^{-1}$; b) flow of oxygen (2 equiv): 10 $mL min^{-1}$, flow of α-terpinene solution: 2 $mL min^{-1}$.

polymer with highest surface area, the reaction proceeded to near complete conversion (96%).

Measurements at a doubled flow rate, (2 $mL min^{-1}$ and half the reaction time), show overall the same trend, with an offset to lower values as expected from the reduced residence time. This indicates that the measurements performed under continuous flow conditions are indeed reproducible.

Although the surface area seems to play an important role in the photocatalytic event as shown by the increased performance of the templated polymers, other effects such as dispersablity and "effective surface area" need to be accounted for. Indeed, the influences of porosity on microarchitectural features are manifold and cannot be easily separated from each other. In any case CMP_0 performed worst, whereas the templated CMPs show highly improved efficiencies.

The polymer networks showed different dispersion stabilities. CMP_0 re-aggregated upon storage in chloroform, whilst CMP_60 was still well-dispersed after the same time (Figure S11 in the Supporting Information). The lower density of CMP_60 can be attributed to the higher surface area and larger pore volume and is the main reason for the stable dispersions. Enhanced dispersability may be responsible for more efficient singlet oxygen production.

Based on conversion and flow rate, productivities were calculated. At a flow rate of 1 $mL min^{-1}$, CMP_0 showed the lowest productivity of 0.03 $mmol min^{-1}$, while polymers with larger surface area reached productivities up to 0.10 mmol min^{-1}. Productivities of up to 0.12 $mmol min^{-1}$ were obtained at doubled flow rate suggesting advantages of using high-surface-area CMPs.

Additionally, tetraphenylporphyrin (TPP) was used as a known sensitizer with high quantum yield at various flow rates and with two equivalents of oxygen.[14] Complete conversion was achieved even at 10 $mL min^{-1}$, corresponding to a productivity of 1.0 $mmol min^{-1}$ and a residence time of

only seconds, thus demonstrating the high efficiency of the continuous flow setup. At even higher flow rates the conversion breaks down, as the photon flow of the light source is becoming a limiting factor ($\Phi_P = 2.5\ mmol\,min^{-1}$). The selectivity of the reaction was not affected by the choice of catalyst, and the endoperoxide ascaridole was formed with a selectivity of 86–88%. Comparison of productivities achieved show that the maximum singlet oxygen quantum yield for the CMPs $\Phi_\Delta = 0.06$ is about one order of magnitude lower than that of TPP. While the polymer network is less productive, the ease of CMP recovery by simple filtration presents a clear advantage. FTIR, thermal gravimetrical and elemental microanalysis of CMP_60 (Table S1 in the Supporting Information) show no modification of the polymer after the photoreaction, thus indicating that it is stable to both irradiation and singlet oxygen.

To demonstrate the reusability of these materials, five repeating experiments of singlet oxygen production were carried out using the same CMP_55 catalyst (Figure S13 in the Supporting Information). The polymer can be reused repeatedly after a simple filtration, and conversions higher than 50% and selectivities above 80% are achieved. The decrease in conversion of 3.6% per run on average can be accounted to photobleaching of the polymer or partial deactivation by singlet oxygen.

To compare our heterogeneous photocatalysts to a homogeneous analogue, singlet oxygen reaction was performed by using the same setup and employing a linear photosensitizer, 4,7-bis(phenylethynyl)benzo[c][1,2,5]thiadiazole (**M1**),[18] which corresponds to the repeating unit of the CMPs under investigation. M1 exhibited almost complete conversion up to substrate flow rates of $10\ mL\,min^{-1}$, thereby proving that indeed the repeat unit within the CMP is responsible for the singlet oxygen generation. However, photobleaching of approximately 31% of this homogenous photosensitizer was determined with UV/Vis spectra taken after the experiment (Figure S4 in the Supporting Information). Additionally, the ^{1}H NMR spectra of M1 also showed the decreasing signals (Figure S5 in the Supporting Information). In comparison, the CMPs are more stable as shown by the repeatability experiments.

In conclusion, we reported a simple method to synthesize conjugated microporous polymer networks with specific electronic properties and pore texture. By using SiO_2NPs, surface areas can be easily tuned without the need for adjusting further parameters. When using this methodology, the BET surface area of the porous polymers can be doubled compared to the network synthesized in the absence of SiO_2NPs. All polymer networks are microporous with pore sizes in the nanometer range. The SiO_2NPs' templating effect contributes to a better accessibility of the micropore system of the CMPs. This simple methodology is an effective way to control the surface area and total micropore volume of different types of CMPs.

We also present here the first example of a photocatalytic application of CMPs for the production of singlet oxygen and relate the photocatalytic effect to the surface area of a series of polymers that are chemically identical. For the highest surface area, substrate conversions above 90% are achieved. The efficiency and reaction rates are however still about one order of magnitude lower than the best homogeneous catalyst.

Nevertheless, this is to our opinion more than compensated by the ease to remove and reuse the catalyst with only a simple filtration, which is especially relevant for sensitive substrates. Also, immediate further consecutive all-in-flow chemistry allows only filtration steps, while cumbersome purification steps are rather inhibitive.

Received: September 4, 2012
Revised: December 3, 2012
Published online: December 18, 2012

Keywords: conjugated microporous polymers · heterogeneous catalysis · polymers · singlet oxygen · surface areas

[1] a) J. X. Jiang, F. Su, A. Trewin, C. D. Wood, N. L. Campbell, H. Niu, C. Dickinson, A. Y. Ganin, M. J. Rosseinsky, Y. Z. Khimyak, A. I. Cooper, *Angew. Chem.* **2007**, *119*, 8728; *Angew. Chem. Int. Ed.* **2007**, *46*, 8574; b) J. X. Jiang, F. Su, H. J. Niu, C. D. Wood, N. L. Campbell, Y. Z. Khimyak, A. I. Cooper, *Chem. Commun.* **2008**, 486–488; c) J.-X. Jiang, F. Su, A. Trewin, C. D. Wood, H. Niu, J. T. A. Jones, Y. Z. Khimyak, A. I. Cooper, *J. Am. Chem. Soc.* **2008**, *130*, 7710–7720; d) J.-X. Jiang, A. Trewin, F. Su, C. D. Wood, H. Niu, J. T. A. Jones, Y. Z. Khimyak, A. I. Cooper, *Macromolecules* **2009**, *42*, 2658–2666; e) J. Weber, A. Thomas, *J. Am. Chem. Soc.* **2008**, *130*, 6334–6335; f) H. Lim, J. Y. Chang, *Macromolecules* **2010**, *43*, 6943–6945; g) J.-X. Jiang, A. Laybourn, R. Clowes, Y. Z. Khimyak, J. Bacsa, S. J. Higgins, D. J. Adams, A. I. Cooper, *Macromolecules* **2010**, *43*, 7577–7582; h) K. Zhang, B. Tieke, F. Vilela, P. J. Skabara, *Macromol. Rapid Commun.* **2011**, *32*, 825–830; i) K. Zhang, B. Tieke, J. C. Forgie, F. Vilela, J. A. Parkinson, P. J. Skabara, *Polymer* **2010**, *51*, 6107–6114; j) Q. Chen, M. Luo, P. Hammershøj, D. Zhou, Y. Han, B. W. Laursen, C.-G. Yan, B.-H. Han, *J. Am. Chem. Soc.* **2012**, *134*, 6084–6087; k) E. Preis, C. Widling, U. Scherf, S. Patil, G. Brunklaus, J. Schmidt, A. Thomas, *Polym. Chem.* **2011**, *2*, 2186–2189; l) R. S. Sprick, A. Thomas, U. Scherf, *Polym. Chem.* **2010**, *1*, 283–285; m) A. I. Cooper, *Adv. Mater.* **2009**, *21*, 1291–1295; n) A. Thomas, *Angew. Chem.* **2010**, *122*, 8506–8523; *Angew. Chem. Int. Ed.* **2010**, *49*, 8328–8344; o) R. Dawson, A. I. Cooper, D. J. Adams, *Prog. Polym. Sci.* **2012**, *37*, 530–563.

[2] N. B. McKeown, P. M. Budd, K. J. Msayib, B. S. Ghanem, H. J. Kingston, C. E. Tattershall, S. Makhseed, K. J. Reynolds, D. Fritsch, *Chem. Eur. J.* **2005**, *11*, 2610.

[3] a) C. D. Wood, B. Tan, A. Trewin, F. Su, M. J. Rosseinsky, D. Bradshaw, Y. Sun, L. Zhou, A. I. Cooper, *Adv. Mater.* **2008**, *20*, 1916; b) J. Y. Lee, C. D. Wood, D. Bradshaw, M. J. Rosseinsky, A. I. Cooper, *Chem. Commun.* **2006**, 2670; c) C. D. Wood, B. Tan, A. Trewin, H. J. Niu, D. Bradshaw, M. J. Rosseinsky, Y. Z. Khimyak, N. L. Campbell, R. Kirk, E. Stockel, A. I. Cooper, *Chem. Mater.* **2007**, *19*, 2034.

[4] a) R. Palkovits, M. Antonietti, P. Kuhn, A. Thomas, F. Schüth, *Angew. Chem.* **2009**, *121*, 7042–7045; *Angew. Chem. Int. Ed.* **2009**, *48*, 6909–6912; b) R. Dawson, D. J. Adams, A. I. Cooper, *Chem. Sci.* **2011**, *2*, 1173–1177; c) J.-X. Jiang, C. Wang, A. Laybourn, T. Hasell, R. Clowes, Y. Z. Khimyak, J. Xiao, S. J. Higgins, D. J. Adams, A. I. Cooper, *Angew. Chem.* **2011**, *123*, 1104–1107; *Angew. Chem. Int. Ed.* **2011**, *50*, 1072–1075; d) L. Ma, M. M. Wanderley, W. Lin, *ACS Catal.* **2011**, *1*, 691–697; e) C. Bleschke, J. Schmidt, D. S. Kundu, S. Blechert, A. Thomas, *Adv. Synth. Catal.* **2011**, *353*, 3101–3106.

[5] L. Chen, Y. Honsho, S. Seki, D. Jiang, *J. Am. Chem. Soc.* **2010**, *132*, 6742 – 6748.
[6] F. Vilela, K. Zhang, M. Antonietti, *Energy Environ. Sci.* **2012**, *5*, 7819 – 7832.
[7] a) R. C. Coffin, J. Peet, J. Rogers, G. C. Bazan, *Nat. Chem.* **2009**, *1*, 657; b) L. J. Huo, J. H. Hou, S. Q. Zhang, H. Y. Chen, Y. Yang, *Angew. Chem.* **2010**, *122*, 1542; *Angew. Chem. Int. Ed.* **2010**, *49*, 1500.
[8] a) S. H. Park, A. Roy, S. Beaupre, S. Cho, N. Coates, J. S. Moon, D. Moses, M. Leclerc, K. Lee, A. J. Heeger, *Nat. Photonics* **2009**, *3*, 297; b) F. Huang, K. S. Chen, H. L. Yip, S. K. Hau, O. Acton, Y. Zhang, J. D. Luo, A. K. Y. Jen, *J. Am. Chem. Soc.* **2009**, *131*, 13886.
[9] P. E. Schwenn, K. Gui, A. M. Nardes, K. B. Krueger, K. H. Lee, K. Mutkins, H. Rubinstein-Dunlop, P. E. Shaw, N. Kopidakis, P. L. Burn, P. Meredith, *Adv. Energy Mater.* **2011**, *1*, 73.
[10] K. Mutkins, K. Gui, M. Aljada, P. E. Schwenn, E. B. Namdas, P. L. Burn, P. Meredith, *Appl. Phys. Lett.* **2011**, *98*, 153301.
[11] a) E. Ji, T. S. Corbitt, A. Parthasarathy, K. S. Schanze, D. G. Whitten, *ACS Appl. Mater. Interfaces* **2011**, *3*, 2820 – 2829; b) S. Chemburu, T. S. Corbitt, L. K. Ista, E. Ji, J. Fulghum, G. P. Lopez, K. Ogawa, K. S. Schanze, D. G. Whitten, *Langmuir* **2008**, *24*, 11053 – 11062.
[12] C. Xing, L. Liu, H. Tang, X. Feng, Q. Yang, S. Wang, G. C. Bazan, *Adv. Funct. Mater.* **2011**, *21*, 4058 – 4067.
[13] M. C. DeRosa, R. J. Crutchley, *Coord. Chem. Rev.* **2002**, *233 – 234*, 351 – 371.
[14] W. Pickenhagen, D. Schatkowski, US Pat. 5892059, **1999**.
[15] J. Wahlen, D. E. De Vos, P. A. Jacobs, P. L. Alsters, *Adv. Synth. Catal.* **2004**, *346*, 152 – 164.
[16] B. A. DaSilveira Neto, A. S. A. Lopes, G. Ebeling, R. S. Gonçalves, V. E. U. Costa, F. H. Quina, J. Dupont, *Tetrahedron* **2005**, *61*, 10975 – 10982.
[17] F. Lévesque, P. H. Seeberger, *Org. Lett.* **2011**, *13*, 5008 – 5011.
[18] G. K. B. Clentsmith, L. D. Field, B. A. Messerle, A. Shasha, P. Turner, *Tetrahedron Lett.* **2009**, *50*, 1469 – 1471.

